Desalination and Water Treatment
www.deswater.com

doi:10.5004/dwt.2017.20414

68 (2017) 49–59
March

Influence of the physical conditions of a xylose and arabinose solution on nanofiltration separation performance

Hetian Liu[a,b], Yang Yang[a,b], Liming Zhao[a,b,*], Hefei Zhao[c], Liqiang Fan[a,b], Lihua Jiang[a], Yongjun Qiu[a,b], Jiachun Zhou[a]

[a]*State Key Laboratory of Bioreactor Engineering, R&D Center of Separation and Extraction Technology in Fermentation Industry, East China University of Science and Technology, Shanghai 200237, China, email: liu.h.tian@foxmail.com (H. Liu), longzaiye@163.com (Y. Yang), Tel. /Fax +86 21 64250829, email: zhaoliming@ecust.edu.cn (L. Zhao), fanglq@ecust.edu.cn (L. Fan), lhjiang@ecust.edu.cn (L. Jiang), qiuyongjun@ecust.edu.cn (Y. Qiu), jczhou@ecust.edu.cn (J. Zhou)*
[b]*Shanghai Collaborative Innovation Center for Biomanufacturing Technology (SCICBT), Shanghai200237, China*
[c]*Shanghai Qiyu Bio-technique Co., Ltd., Shanghai 200235, China, email: vichefei@163.com (H. Zhao)*

Received 20 June 2016; Accepted 9 December 2016

ABSTRACT

To evaluate the feasibility of isomer separation by nanofiltration (NF), the effects of different monosaccharide stereo-structures on separation performance of xylose and arabinose nanofiltration were studied in this work. An NF250 membrane was used to study xylose and arabinose rejection under different physical conditions. The retention differences between xylose and arabinose were investigated under different solution conditions during NF processing. Furthermore, the influences of physical conditions on molecular computational radius (r_c) and diffusion coefficient of the solute (D_p) were analyzed. The STERIMOL model was introduced to describe the theoretical sizes of monosaccharide molecules. D_p was applied to calculate the degree of rejections. The results showed that the rejection ratio of xylose to arabinose increased as D_p exceeded 5.0. Maintaining the trans-membrane pressure (TMP) between 8.0 and 12.0 bar, elevating the operation temperature and reducing the concentration of the bulk solution helped increase the rejection ratio of xylose to arabinose. This study presents a potential approach for monosaccharide isomers separation by solution physical properties regulating.

Keywords: Nanofiltration; Arabinose; Xylose; Stereo-structure; Molecular computational radius

1. Introduction

Pentoses such as xylose and arabinose are important monosaccharides that are essential nutritional supplements in the food processing industry. Pentoses for commercial purpose can be extracted from natural carbohydrate polymers such as semi-cellulose via hydrolysis followed by enzymatic transfer or through fermentation. Pentoses obtained using these methods are usually mixtures consisting of more than one type of monomer. Isolation of the targeted monosaccharide from others requires a separation procedure. The separation method commonly used for monosaccharides is based on chromatography [1,2]. However, technical challenges, such as appropriate selection of the stationary phase and analytical parameters used for chromatography, render this approach difficult to implement over a wide range of industrial applications [3]. Alternatively, monosaccharide mixture separation and purification could be performed by NF. Sjöman et al. [4] studied the feasibility of separation xylose from glucose by NF, and investigated the influences of operating pressure, concentration, the mass ratio of xylose to glucose et al. different factors on separation effect. Actually, based on the traditional viewpoint, membrane filtration would require a decade difference in molar mass to be able to separate compents from eath other [5], it is rather difficult for isomer separation by NF. However, as

*Corresponding author.

the properties and steric conformations of monosaccharide molecules differ according to their acid–base properties and solution concentration, different treatment methods may be required in NF separation. Liu et al. [6] studied six kinds of monosaccharides and found that rejections of them had existed difference between each other even though those monosaccharides were isomers.

In order to achieve better separation effect, different physical conditions, i.e., temperature, operating pressure, concentration, pH and ion strength, were adjusted in the process of NF separation. NF is a pressure driven separation technology between reverse osmosis and ultrafiltration [7]. Therefore, the operation pressure always plays crucial role on separation performance. Goulas et al. [8] thought the pressure increment leads to increased solvent flux and membrane compaction. Temperature and concentration will affect solution viscosity that lead to the phenomenon of concentration polarization. Furthermore, the polymer of membrane material will reorientate due to an increasing in flexibility of molecular chains with increasing temperature [9]. pH and ion strength will also lead to the change of membrane charge [10]. Weng et al. [11] found that acetic acid could be better separated from xylose by Desal-5 DK membrane depending on changing the solution pH. However, the influence of solute concentration, pH, filtration pressure and temperature on the solute conformation is vague. Therefore, it is extreme important to research the influence of physical conditions on solute molecular conformation.

As for neutral solutes, the permeance of solutes are controlled by sieving effect, and the differences of separation mostly exist in molecular sizes and diffusivities [11]. Saccharides, for instance, xylose, lactose, glucose and sucrose [12–19], are typical neutral solutes often utilised to test the separation performance and determine the pore size of NF membranes. Few references with data on the NF separation of different saccharides of equivalent MW are available. Monosaccharide isomers are known to exist naturally in plants. Therefore, separation of isomers must be considered in monosaccharide extraction procedure. Data in Table 1 show that the reflection coefficient (σ) of arabinose is higher than that of xylose, which implies that arabinose retention on the NF membrane must be higher than that of xylose [20] on the same membrane with a MWCO of 150 Da; in fact, the retention difference between these pentoses is about 10%. Solute permeation effects reflect steric or molecular sieving effects and are influenced by interactions between solute and pore wall (membrane materials) [21].

Table 1
Physical characteristics of arabinose and xylose

	l-Arabinose	d-Xylose
Molecular weight (g/mol) [7]	150.13	150.13
Reflection coefficient [18]	0.895	0.776
Dissociation constants value (pKa) [29]	12.34	12.15
Equivalent molar diameter (nm) [11]	0.68	0.65
Specific rotation	+103.3°	+19.0°
Hydration numbers in aqueous solution (298 K) [30]	7.6	6.8

The present study investigates retention differences between xylose and arabinose under different solution conditions during NF processing. Ulteriorly, the influences of physical conditions on molecular computational radius (r_c) and diffusion coefficient of the solute (D_p) were analyzed. A model was constructed to describe the relationships amongst these parameters, including TMP, temperature and concentration. That would provide theoretical reference for separation of xylose and arabinose. The feasibility of using NF for separating monosaccharide isomers was also evaluated.

2. Theoretical background

2.1. NF membrane flux and rejection

The NF process is driven by TMP. Solute permeation is controlled by diffusion and hindered by convective transport, which could be summarised as in Eq. (1) [22].

$$J_s = J_v C_p = -D_p \frac{dC}{dx} + J_v K_c C \tag{1}$$

where J_s is the solute flux, J_v is the bulk solution flux, C_p is the permeate concentration, D_p is the diffusion coefficient of the solute and K_c is the hindrance factor for convection.

According to the Hagen–Poiseuille equation, which is normally used in capillary mechanics, J_v in the pore model may be expressed as follows [22–24].

$$J_v = \frac{r_p^2(\Delta P - \Delta\pi)}{8\eta\Delta x} \tag{2}$$

$$\Delta P = \frac{P_{in} + P_{out}}{2} \tag{3}$$

where ΔP refers to the Trans-membrane pressure (TMP), which could be calculated as the mean of the inlet and outlet membrane pressures as shown in Eq. (3) [20], D_p is the difference between the inlet and outlet pressures, also called the osmotic pressure difference, dx is the length of the pore, r_p is the effective pore size and η is the viscosity of the bulk solution under the given operating conditions.

Based on a study of Bruggen and Wang [25,26], a relationship between r_p and molecular weight cut-offs (MWCO) of the NF membrane may be obtained.

$$MWCO = 1798.3rp^{2.3168} \tag{4}$$

Bowen et al. [22] proved that solute concentrations at the inlet and outlet sides of a membrane may be expressed by the bulk and permeate concentrations as well as the steric partition factor. This relationship may be generalised as follows.

$$C_i = \Phi C_f \tag{5}$$

$$C_o = \Phi C_p \tag{6}$$

where C_i and C_o are the solute concentrations of the inlet and outlet sides of the membrane, respectively, Φ is the steric partition factor and C_f is the feed concentration of the bulk solution.

The parameter Φ is better known in membrane science as the molecular sieving factor. Uncharged organic compounds are not spherical; therefore, Φ may be affected by molecular shapes. The parameters L and molecular width (*MWd*) were obtained from the STERIMOL parameters [27] that normally used in pharmacy. The line linking the two atoms with the longest distance amongst the molecules was defined as the L-axis. The distance between A and B, as shown in Fig. 1, is defined as L. Other atoms in this molecule then project to the perpendicular plane of the L-axis. The smallest rectangle that can encompass all projections is then created. Vertical lines are drawn on both sides of this rectangle from the centre of the molecule. The four parameters obtained were defined as B_1 to B_4 in STERIMOL model. To avoid excessive numbers of parameters, the area of this rectangle was designated as S to replace B_1 to B_4.

Yoshiaki integrated a series of functions between Φ and r_p based on the model above [21]. These functions can be summarised as the following equations:

$$\Phi = \int_0^{\frac{\pi}{2}} \frac{\left(\sqrt{{r_p}^2 - \left(\frac{L\cos\alpha + \sqrt{S}\sin\alpha}{2}\right)^2} - \frac{\sqrt{S}}{2}\right)^2}{{r_p}^2} p(\alpha) d\alpha \tag{7}$$

$$\int_0^{\frac{\pi}{2}} p(\alpha)\, d\alpha = 1 \tag{8}$$

Solute rejection was summarised by C_p and C_f as in Eq. (9) and in Eq. (10).

$$R_{j(cal)} = 1 - \frac{C_p}{C_f} \tag{9}$$

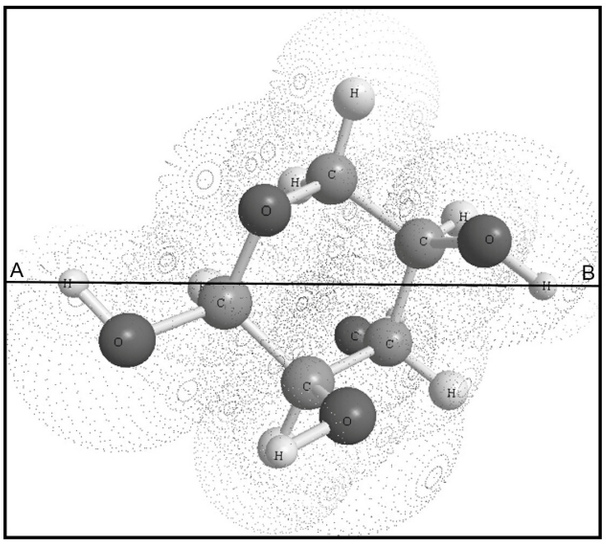

Fig. 1. Model of molecular length (L).

$$R_{j(cal)} = 1 - \frac{\Phi K_c}{1 - (1 - \Phi K_c)\exp(-Pe)} \tag{10}$$

Pe is the Péclet number [28] which is defined as follows.

$$Pe = \frac{K_c J_v \Delta x}{D_p} \tag{11}$$

K_c, as the hindrance factor, could be calculated from the ratio of the solute radius to the pore radius (l) and the hydrodynamic coefficient *G(l)*. Bowen reported this hydrodynamic coefficient in 2002 [23,24].

$$K_c = (2 - \Phi) G(\lambda) \tag{12}$$

$$G(\lambda) = 1.0 + 0.054\lambda - 0.988\lambda^2 + 0.441\lambda^3 \tag{13}$$

$$K_d = 1.0 - 2.30\lambda + 1.154\lambda^2 + 0.224\lambda^3 \tag{14}$$

$$\lambda = \frac{r_c}{r_p} \tag{15}$$

2.2. Molecular computational radius (r_c)

The parameters of Eq. (10) were calculated by the molecular shape parameters L and *MWd* and the pore-size model of log-normal distribution, wherein *MWd* [21] and its distribution function are defined as follows.

$$MWd = \frac{r_c}{1.42} + 1 \times 10^8 \tag{16}$$

$$f(r_p) = \frac{1}{r_p \sigma_y \sqrt{2\pi}} \exp\left[-\frac{\left(\bar{y} - y\right)^2}{2{\sigma_y}^2}\right] \tag{17}$$

In the present work, we calculated the pore size of the NF membrane based on the uniform pore-size model. Thus, the mean of the logarithm of (r_p – b) (which is designated as $\bar{y}$) should have the same value as y and the lower limit of r_p should be equal to r_p. Based on this assumption, Eq. (17) could be simplified to

$$f(r_p) = \frac{1}{\sqrt{2\pi} r_p \sigma_y} \tag{18}$$

where s_y is the standard deviation of y, which could be expressed as follows based on Yoshiaki's work [21].

$$\sigma_y = \ln\left(\frac{{r_p}^2 + {\sigma_p}^2}{{r_p}^2}\right) \tag{19}$$

where s_p is defined as the standard deviation of p.

Eq. (1) should be approximated according to the uniform pore-size model. The rejection (R_j) could be expressed by the following equations:

$$C_p = \frac{\bar{J}_s}{\bar{J}_v} = \frac{\int J_s(r) f(r) dr}{\int J_v(r) f(r) dr} \tag{20}$$

In the uniform pore-size model, s_p could be zero. Integrating Eq. (16) to Eq. (19), a mathematic relation could be summarized as Eq. (22).

$$J_s = \frac{D_p}{\Delta x}\left(C_f - C_p\right) + J_v K_c \sqrt{C_f C_p} \tag{21}$$

$$R_j = 1 - \frac{8\eta D_p R_j + r_p^2\left(\Delta P - \Delta\pi\right)K_c\sqrt{1-R_j}}{r_p^2\left(\Delta P - \Delta\pi\right)} \tag{22}$$

In this work, the values of R_j were equal to observed rejections. Thus, r_c could be calculated by Eq. (22).

2.3. Relationships between diffusivity and feed solution parameters

D_p in Eq. (1) is defined as the diffusion coefficient of the solute in a pore of the NF membrane. This parameter could be expressed in terms of Eq. (23) as follows.

$$D_p = K_d D \frac{\eta}{\eta_0} \tag{23}$$

where K_d is hindrance factors for diffusion.

As shown by Bowen [22], the η of water increases inside a membrane pore. Therefore, the following function was constructed.

$$\frac{\eta}{\eta_0} = 1 + 18\left(\frac{d}{r_p}\right) - 9\left(\frac{d}{r_p}\right)^2 \tag{24}$$

where η and η_o are the viscosities of the solution and water, respectively, and d is the thickness of one water molecule (d = 0.28 nm).

In Yoshiaki's approach [21], the relationship between the diffusivity and molecular Stokes radius can be presented as follows. However, the molecular Stokes radius would be replaced by r_c in this work.

$$D = \frac{k\left(T + 273\right)}{6\pi\eta \times 10^3} \times \frac{1}{r_c} \tag{25}$$

where k is the Boltzmann constant (k = 1.38065 × 10^{-23} *J/K*), r_c is the molecular computational radius and T is the operation temperature.

3. Materials and methods

3.1. Chemicals and reagents

D-Xylose (>99%) and L-arabinose (>99%) were purchased from Shanghai Tianlian Fine Chemical Co., Ltd. Calcium sulphate and sodium ethylenediaminetetraacetic acid (EDTA) were supplied by Sinopharm Chemical Reagent Co., Ltd. Magnesium sulphate heptahydrate and acetic acid were obtained from Lingfeng Chemical Reagent Co., Ltd. (Shanghai) and sodium hydroxide was obtained from Titanchem Co., Ltd. EDTA calcium disodium salt hydrate was supplied by Sigma–Aldrich Co., Ltd. (Shanghai). The chemical reagents listed above were of analytical-reagent grade. Deionised water was generated for experimental and cleaning purposes using a reverse osmosis membrane. Ultrapure water for pentose detection (conductivity ≤ 12 μs cm^{-1}) was prepared by ion exchange (Shanghai Huazhen Co., Ltd.). Syringe filters in the aqueous phase for filtration of the solution were purchased from RephiLe Bioscience, Ltd. The filter pore diameter was 0.45 μm.

3.2. Properties of xylose and arabinose

The MWs and equivalent molar diameters of xylose and arabinose are both the same. Theoretically, these molecules that have identical size cannot be separated by an NF membrane based on sieve effects. The chemical configurations of selected pentose in solution vary: arabinose is an L-type molecule, whereas xylose is D-type. The cyclic structures of both molecules are pyranose-like in nature. The physical characteristics of arabinose and xylose were shown in Table 1.

3.3. NF membrane

The NF membrane (QY-NF-3-D) was a membrane composite NF module obtained from Shanghai Qiyu Bio-technique Co., Ltd. The MWCO of the NF membrane was 250 Da. The NF membrane was made of aromatic polyamides and featured an effective surface area of 0.20 m^2. The maximum pressure tolerance of the membrane was 25 bar, and its maximum tolerable T was 40°C. The operational pH of this membrane varied from 2.0 to 12.0.

3.4. Solution condition adjustment

TMP, T and solution concentration were varied to study NF retention differences between the two pentoses; these conditions may affect the steric conformations and other physicochemical properties of the solutes. NF experiments with different solution conditions and TMP were conducted to evaluate retention differences.

About 6L of syrup for three batches was prepared; 2 L of this syrup was used as the feed solution for each batch. TMP ranged from 2.5 bar to 20.0 bar, T varied at 15, 18, 21, 24, 27, 30, 33 and 36°C and the pH of the syrup was regulated by acetic acid and sodium hydroxide to obtain values of 5.0, 6.0, 7.0, 8.0 and 9.0. The solute concentrations of xylose and arabinose were adjusted to 6, 10, 20, 30 and 40% (w/v). Here, 6% (w/v) is defined as 6 g per 100 mL; all other remaining concentrations were defined in the same manner. The pentose syrup was mixed and dissolved only once before immediate preservation at 4°C in a refrigerator to maintain equivalent initial concentrations and experimental conditions.

3.5. Analytical methods

NF experiments were run under different conditions as described above to evaluate the relationship between retention, flux of permeation and operating conditions. Permeate and retentate samples were collected and analysed by HPLC to calculate the concentration of each individual component.

An Agilent HPLC system was used to measure the concentration of each pentose. The system was equipped with a Waters (USA) Sugarpak-I column with a diameter, length and pore size of 6.5 mm, 300 mm and 10 μm, respectively, and a RID detector. The mobile phase used was ultrapure water (conductivity ≤ 12 μs cm^{-1}) flowing at a rate of 0.5 mL min^{-1} at 80°C. The sample injection volume was 10 μL. Standard samples were prepared by serial gradient dilution of the individual stoke solutions to afford pentose concentrations of 0.5, 1, 2, 4, 6 and 8 g L^{-1}. Calibration generally yielded standard curves with coefficients of determination (R^2) greater than 0.99 within the range of experimental concentrations examined. Matlab, Chem Office and Hyperchem software were used to calculate distances between atoms and molecular computational diameters of the monosaccharide molecules.

A Brookfield LVDV-II+P viscometer was used to measure the η of different solutions under different physical conditions. Rotor #0 was selected based on the range of η. The rotation speed was set to a minimum of 6 rpm.

4. Results and discussion

4.1. Influence of pressure on xylose and arabinose separation

Fig. 2(a) illustrates the retention of each pentose in solution without pH and ionic strength regulation. The deionised water used in the experiments was subacidic and showed a pH of approximately 6.0. The pH of the syrup was 5.1. The scedastic line obtained demonstrates very good agreement amongst results obtained between 2.0 and 20.0 bar. As shown in Fig. 2(b), the rejection ratio of arabinose to xylose decreased as the pressure increased from 2.0 bar to 5.0 bar then remained constant beyond 5.0 bar. The highest ratio was obtained at 2.0 bar. However, the rejections of arabinose and xylose were too low for easy observation at this ratio. From 5.0 to 10.0 bar, rejection ratios of arabinose to xylose were below the value at a higher TMP which indicates that pressures in the stable stage from 12.0 bar to 18.0 bar may be appropriate for the experiments. The rejection ratio of arabinose to xylose profile in Fig. 2(b) shows a slightly decline from 1.21 to 1.18. Over this TMP, the rejection ratio maintained a temporarily stable level of 1.20. Meanwhile, The statistical analysis of rejection with pressure was done by the process of One-Way-ANOVA and the result showed that the rejection is not statistically significant with the pressure ($P = 0.947 > 0.05$). Thus, to avoid possible damage to the NF equipment caused by high pressure, 12.0 bar was considered the most suitable TMP for subsequent experiment.

4.2. Influence of temperature and pH on xylose and arabinose separation

Fig. 3(a) and 3(b) showed that the rejection of each pentose decreased as T increased. That may be due to the change of solution viscosity under different temperature. Fig. 3(c) showed the relationship between T and ratios of rejection for arabinose and xylose at each pH. The rejection data showed more significant differences at a TMP of 12.0 bar, T of 21°C and pH of 9.0 than under other solution conditions. Actually, solute rejection will be influenced by temperature and pH of solution. Except for the effect of physical conditions on membrane, the molecular structure also will be changed. For example, the proportion of furan ring of pentose will change with temperature [31].

Rejection of xylose and arabinose presented a discrepancy that rejection of xylose ranges from 0.4 to 0.6, while arabinose rejection ranges from 0.5 to 0.7. Equivalent molar diameter listed in Table 1 could show an explanation for the difference of rejection. Arabinose has the equivalent molar diameter of 0.68 nm which is slightly bigger than xylose of 0.65 nm. Molecular stereo structure will change with the change of bond angles in feed solution especially under different TMP during NF process. Equivalent molar diameter is the basis of this discrepancy. Bigger diameter leads to the bigger rejection in NF process.

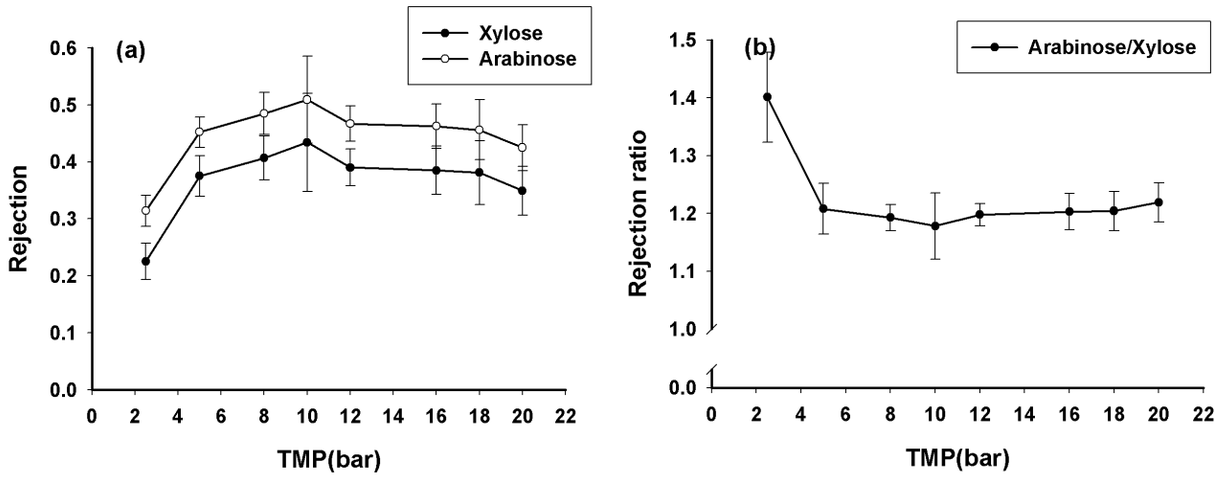

Fig. 2. (a) Rejection of arabinose and xylose as a function of TMP. (b) Rejection ratio of arabinose to xylose as a function of TMP. The concentration of each pentose in the original solution was maintained at 3% (w/v), the operating temperature was held at 25.0 ± 0.5°C and the solution pH was maintained at 5.1 ± 0.1.

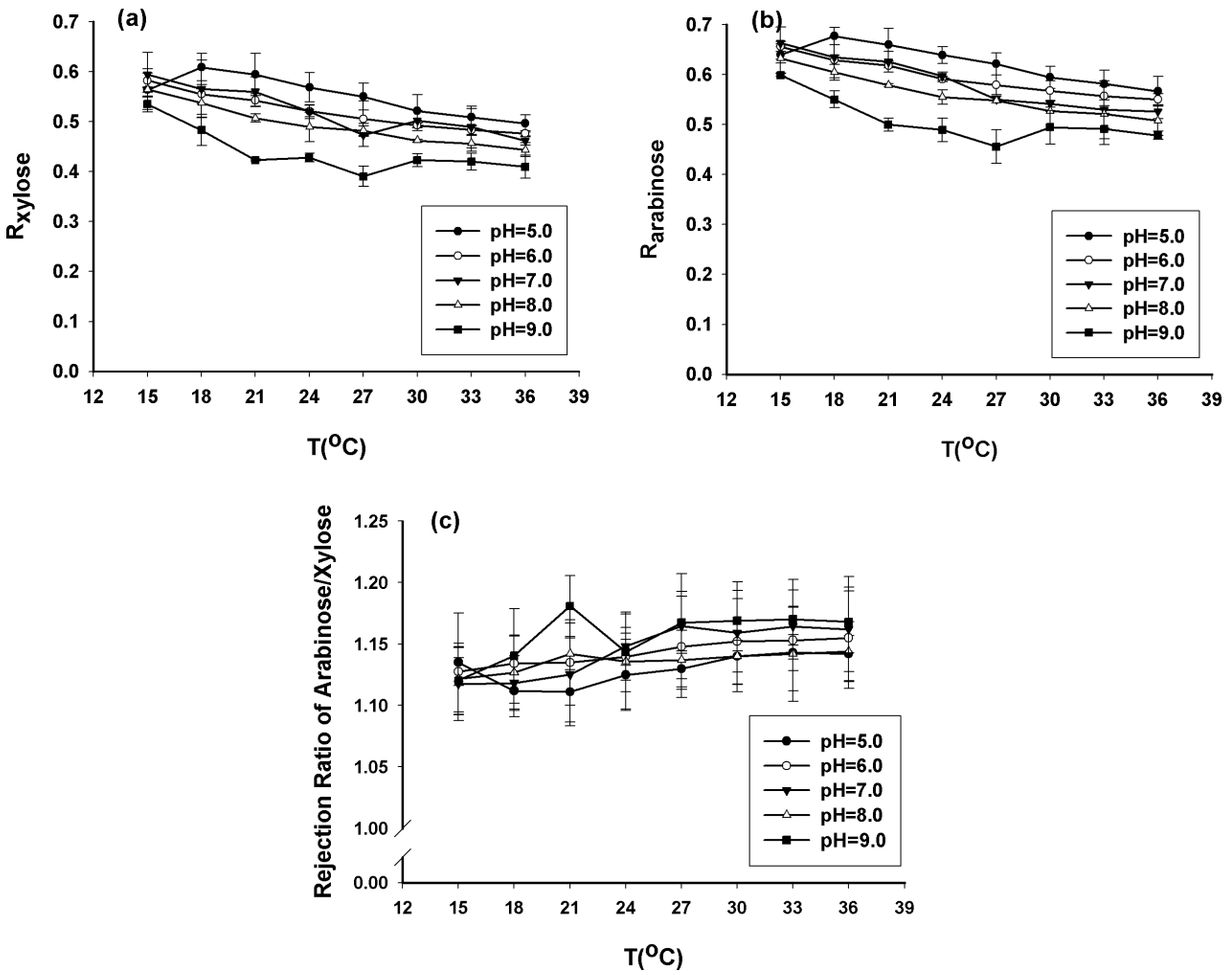

Fig. 3. (a) Rejection of xylose at different pH as a function of temperature. (b) Rejection of arabinose at different pH as a function of temperature. (c) Rejection ratio of arabinose to xylose at different pH as a function of temperature. The TMP was held at 12.0 bar, the concentrations of xylose and arabinose were maintained at 3% (w/v) and the solution pH was 5.1.

As shown in Fig. 4, we can find the influence that different temperature on xylose and arabinose molecule. The dominant ring structure in xylose and arabinose both contain four hydroxyl groups. These hydroxyl groups distribute in the stereo space with the type of axial bond and equatorial bond. The lowest molecular energy of xylose and arabinose molecules would change with the temperature of the solution during NF process. Hyperchem and Chem office softwares were used to construct the molecular stereo structures of minimal energy in different solution physical conditions.

Fig. 4 illustrated the ball-and-stick model of xylose and arabinose at 15°C and 36°C. Molecule structures in other conditions were not listed. In Fig. 4, the maximum atoms distance could be seen as the major axis of xylose decreased from 7.75 Å (Å = 10^{-10} m) to 5.48 Å at the temperature increased from 15°C to 36°C. Similarly, arabinose molecule is with the same trend. The major axis decreases from 5.67 Å to 5.65 Å. Blue imaginary line in Fig. 4b and 4d is the possible intramolecular hydrogen bond which could be the influence factor of molecular stereo structure changes.

Based on the theoretically deduced formulas in Section 2.2, we can describe the relationship between solute rejection and η, which could substitute the physical parameters of the solution. In the next series of experiments, we studied the relationship between η and pH. Solutions of the same concentration and *T* but different pH have nearly identical η. In succeeding experiments, we considered a constant pH for calculations and modelling.

4.3. Viscosity model for T and C_s

The parameter η is correlated with *T* and monosaccharide concentration (C_s). We designed experiments to show that different monosaccharides may have the same η at the same *T* and C_s. This trend also applies to bulk solutions with different pH values. Based on these results, experiments were implemented to determine the relationships between η, *T* and C_s.

We determined η over *T* ranging from 20°C to 55°C at intervals of 5°C. Solutions with concentrations (w/v) from 0% (deionised water without any solute) to 80% at intervals of 10% were prepared.

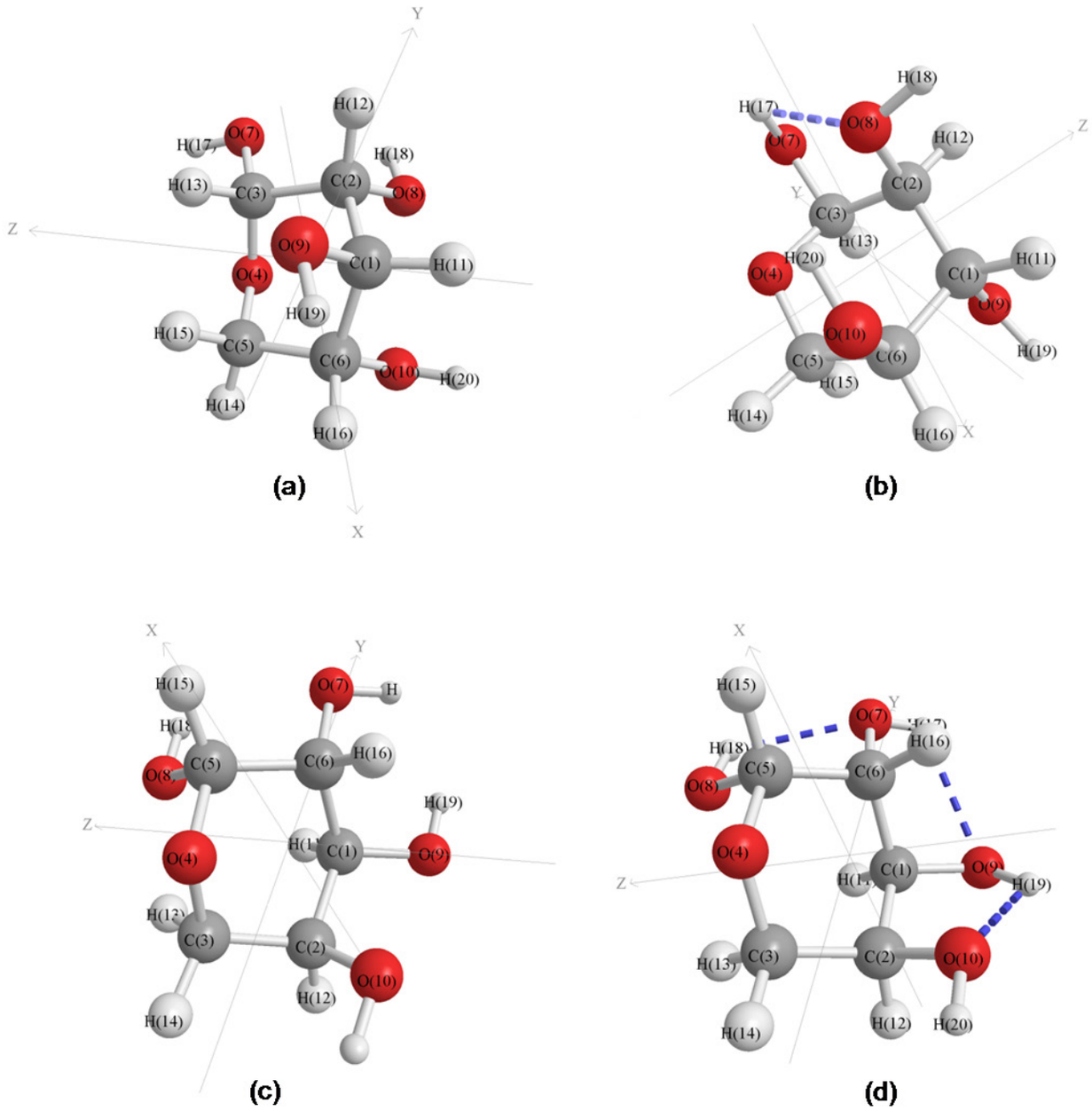

Fig. 4. Ball-and-stick models of xylose and arabinose in the solution, operation solution pH was 9.0. (a) is xylose under temperature of 15°C; (b) is xylose under temperature of 36°C; (c) is arabinose under temperature of 15°C; (d) is arabinose under temperature of 36°C. No additive anion or cation was in the solution.

Geometric fitting curves of the specified solute concentrations were created from the η and T data. The relevant model could be expressed as follows.

$$\eta = a^* T^{b^* T} \tag{26}$$

where a^* and b^* are coefficients which had been listed in Table 2. The solute concentration could be related to these coefficients to obtain the relationship between η, T, C_s and Cs'.

The coefficients could be calculated for C_s with the following equations.

$$a^* = \frac{1.37 + 4.13C_s}{1 + 0.443C_s - 59.1C_s^2} \quad (R^2 = 0.995, N = 9) \tag{27}$$

$$b^* = -\left(0.435 + 3.50Cs - 7.26Cs^2 + 3.82Cs^3\right) \times 10^{-2} \quad (R^2 = 0.958, N = 9) \tag{28}$$

4.4. Analysis of model accuracy

Based on Eq. (22), we calculated the molecular radii (r_c) under different physical conditions based on the rejections observed. Calculated rejections were obtained via another series of equations expressing the original relationship of NF rejection as summarised in Eq. (10).

According to the three-dimensional model constructed by Chem Office, the *L* values of xylose and arabinose in the STERIMOL model were 5.26 Å and 5.66 Å, respectively, and the long sides of the rectangle reflected by other atoms to the *V*-perpendicular plane of the *L*-axis were 5.07 Å and 5.18 Å, respectively. Comparison of these two distances for each pentose indicated that a xylose molecule is more spherical than an arabinose molecule. STERIMOL model is generally used in pharmacy to relate the atom distances of neutral molecules to replace spherical molecular diameters. The width difference between monosaccharide MW was considered and an evaluation for the effectiveness was established. Fig. 5 presents plots of the two correlation equations obtained. The slope which approximate 1.0 indicated that the rejection obtained matched better with the rejection calculated and the STERIMOL model matched closer with the real situation. The slope of each equation demonstrates that the simulation results of xylose are higher than those of arabinose. Considering our STERIMOL model assumption and the similarity of *L* and distances of *L*-axis *V*-perpendicular plane in one molecule, the more approximately spherical a molecule is, the higher its level of simulation determined by the mathematic model in this study.

4.5. Effects of solute concentration on molecular computational radius

High solute concentrations could lead to high η in the bulk solution. During NF, the membrane flux was too low to detect. Considering the requirement of accuracy, an experiment involving solutions with concentrations ranging from 3 g/100 mL to 40 g/100 mL was designed. As shown in Fig. 6, the r_c of both xylose and arabinose presented a downward trend with increasing solute concentration. Decreases in r_c range were more obvious for arabinose than for xylose. The r_c of arabinose was higher than that of xylose at low solute concentrations, which indicates the ease by which structural changes in arabinose may be performed. The Φ we calculated of arabinose (2.03×10^{-2}) was lower than that of xylose (3.75×10^{-2}), which implies a shallower slope of its C_s–r_c curve, contrary to the data of the research.

The stereo formulas of the two pentoses that obtained by Chem Draw software are illustrated in Fig. 6. Compared with the image in Figs. 6 (a) and 6 (b) shows an unstable hydroxyl group which specific applying to the uncertainty configuration of hydrogen bond connected to the carbocycle between *R* and *S* configurations. Structure of arabinose is more stable than that of xylose due to the uncertainly configured hydrogen bond. Φ of arabinose should be higher than that of xylose based on the stability discussed above; however, experimental data presented an opposite relationship. These gave us a message that solute concentration has a more significant impact on xyloses which lead to a higher steric partition factor while changing of C_s.

Table 2
Parameters of the relationship between solution viscosity and conductive temperature

Cs′ (g/100 mL)	0	10	20	30	40	50	60	70	80
Cs (10^3 *mol* m^{-3})	0	0.667	1.33	2.00	2.67	3.33	4.00	4.67	5.33
*a**	1.27	1.90	2.47	3.15	4.99	4.76	6.54	12.7	24.0
*b** (×10^{-3})	–4.33	–8.10	–9.36	–8.91	–7.89	–5.35	–4.77	–5.89	–7.60

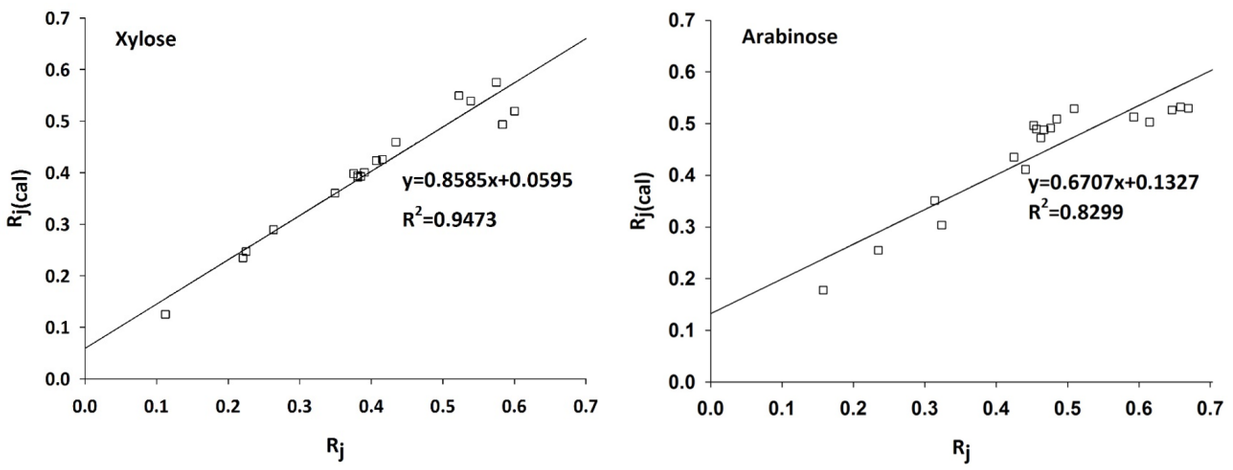

Fig. 5. Observed (R_j) and calculated ($R_{j(cal)}$) rejections of xylose and arabinose at different physical conditions of the solution. TMP ranged from 2.5 bar to 20.0 bar, *T* ranged from 15°C to 36°C and concentration ranged from 6 to 40% (w/v).

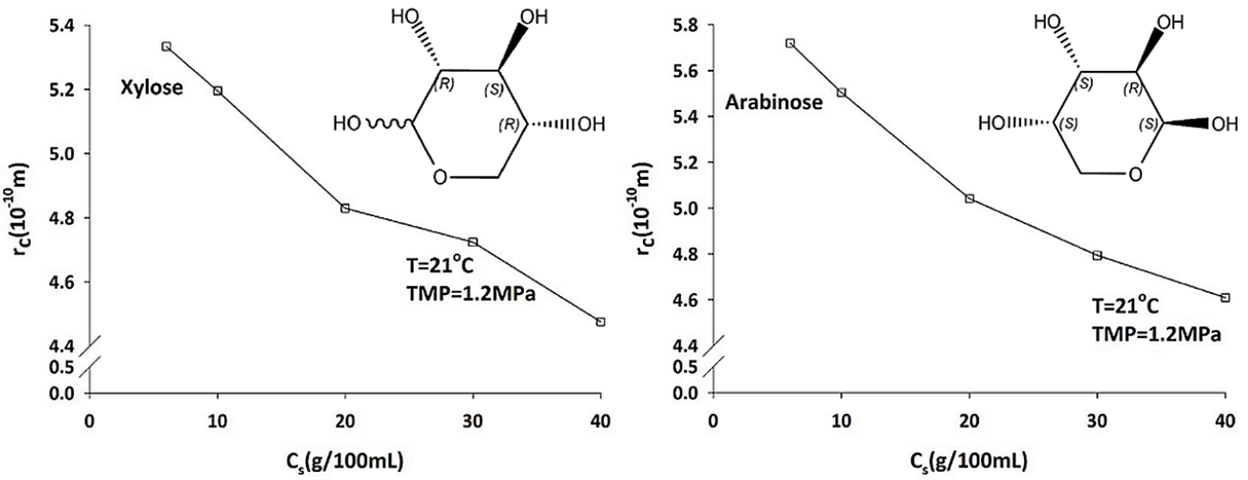

Fig. 6. Relationship between solute concentration and molecular computational radius of xylose and arabinose. The temperature was controlled to 21°C, TMP was 1.2 MPa (12.0 bar) and solution pH was approximately 5.1.

4.6. Expanding separation discrepancy assumption

The rejection and analytical data obtained show potential separation by regulation of bulk solution conditions. Fig. 7 presents the tendency of separation at high D_p. Xylose and arabinose showed nearly identical calculated rejections when D_p was less than 5 $m^2 s^{-1}$. As the D_p increased to values greater than 5, the rejection difference between xylose and arabinose became more obvious. We noted the respective relationships of D_p with TMP, T and C_s, which are illustrated in Fig. 8. D_p presents different relationships with these three parameters. The maximum value of D_p was reached when TMP was nearly 10.0 bar; D_p increased as TMP approached 10.0 bar. With increasing T of the bulk solution, D_p continuously increased. The relationship between solute concentration and D_p presented a type of crosscurrent. To achieve efficient separation, measures to increase D_p must be adopted. Ensuring that TMP is 8.0–12.0 bar, increasing the T within the scope of the equipment capacity and reducing the solute concentration are also effective measures to increase D_p.

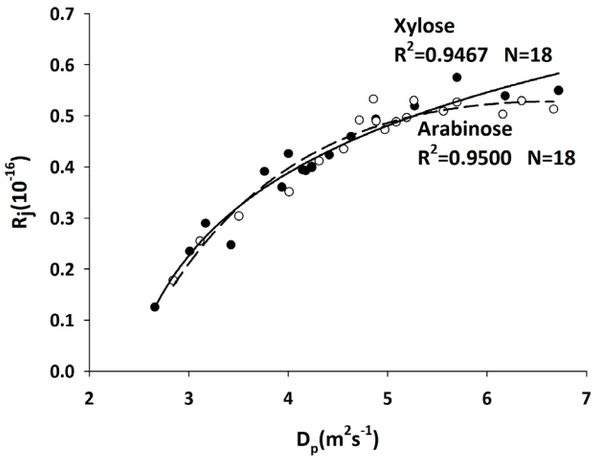

Fig. 7. Relationship between D_p and $R_{j(cal)}$.

5. Conclusions

Molecular shape parameters introduced by the STERIMOL model and membrane pore size were incorporated into the formula for NF rejection to calculate the r_c. The observed rejection corresponded well to the calculated rejection. We expressed the r_c in terms of solution conditions, namely, T, solute concentration and TMP. A relationship between bulk η, solute concentration and T was established.

The r_c of arabinose is more easily changed than that of xylose under different bulk solution conditions, which indicates that the more spherical a molecule is, the more difficult it is to adjust rejection by NF. Change of bond angles and intramolecular hydrogen bonds could be influence factors to molecular stereo structure in different physical conditions of solution, which we will do further explanation in our another research.

The results obtained in this study provide some measures by which to increase rejection differences between xylose and arabinose. These measures include maintenance of TMP at 8.0–12.0 bar, increases in T and decreases in C_s. These measures present a potential approach for separating monosaccharide isomers such as xylose and arabinose.

Symbols

B — lower limit of r_p (m)
C — solute concentration in the pore (mol m^{-3})
C_f — feed concentration (mol m^{-3})
C_i — solute concentration at inlet of membrane (mol m^{-3})
C_o — solute concentration at outlet of membrane (mol m^{-3})
C_p — permeate concentration (mol m^{-3})
C_s — solute concentration in bulk solution (mol m^{-3})

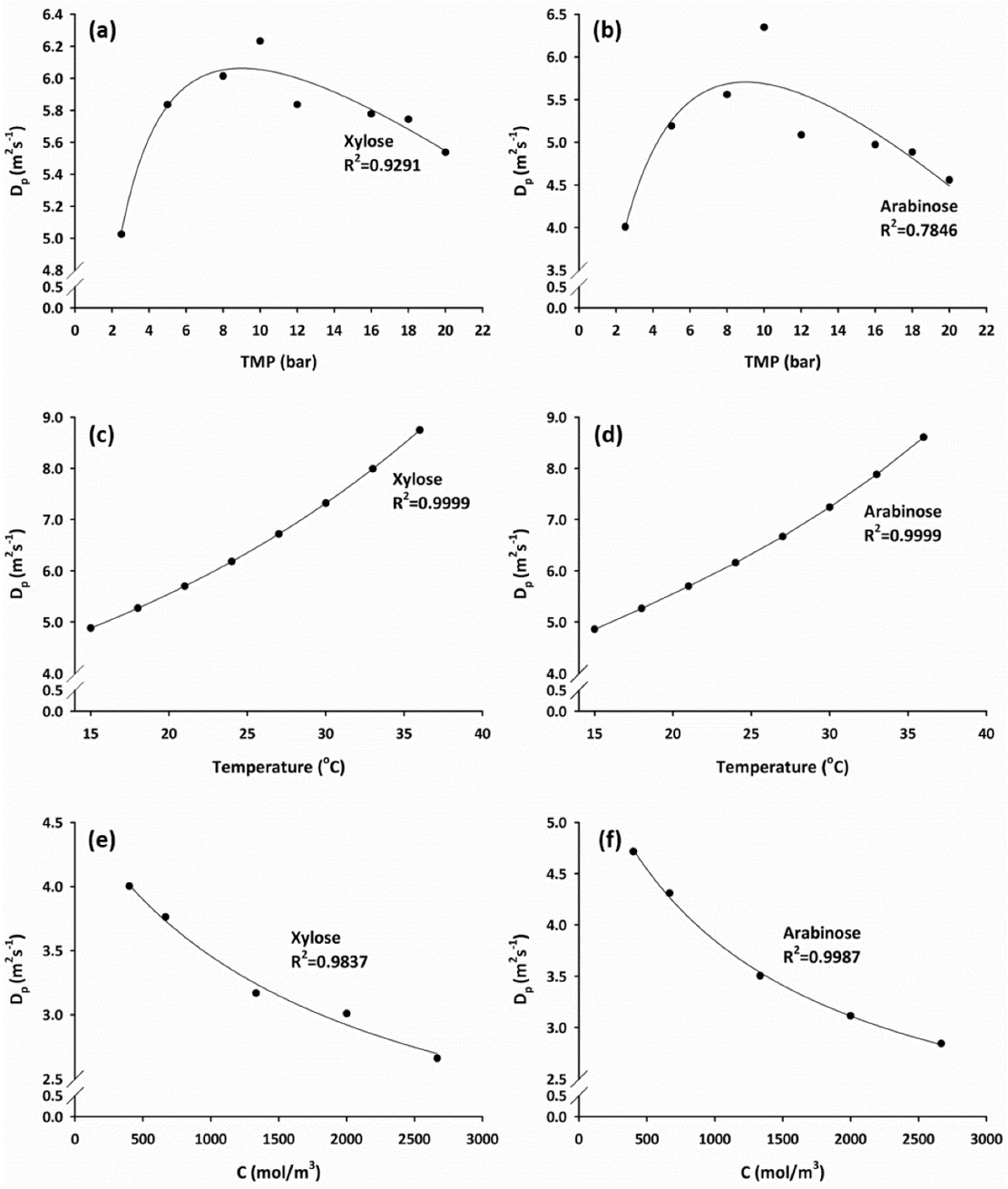

Fig. 8. Relationships between D_p and (a, b) TMP, (c, d) operation temperature and (e, f) solute concentration. (a), (c) and (e) refer to the respective relationships of xylose whereas (b), (d) and (f) refer to those of arabinose.

C_s' — solute concentration in bulk solution (g/100 mL)
D — diffusivity in bulk solution ($m^2\ s^{-1}$)
D — diameter of one water molecule (d = 0.28 nm)
D_p — hindered diffusivity with modification of viscosity ($m^2\ s^{-1}$)
$f(r_p)$ — probability density function of r_p
G — lag coefficient
J_s — solute flux (mol $m^{-2}\ s^{-1}$)
J_s — mean solute flux (mol $m^{-2}\ s^{-1}$)
J_v — water flux ($m^3\ m^{-2}\ s^{-1}$)
J_v — mean water flux (mol $m^{-2}\ s^{-1}$)
K — Boltzmann constant (J K^{-1})
K_c — hindrance factor for convection
K_d — hindrance factor for diffusion
M_p — membrane rejection molecular weight (Da)
MWd — molecular width (m)
Pe — Péclet number
r_c — molecular computational radius (m)

R_j — observed rejection
$R_{j(cal)}$ — calculated rejection
r_p — effective pore radius (m)
T — temperature (°C)
X — position in a pore from inlet (m)
Y — $log\ (r_p - b)$
y — mean of $ln\ y$
ΔP — applied pressure (Pa)
Δx — pore length (m)
$\Delta\pi$ — osmotic pressure difference (Pa)
η — viscosity of water in a pore (mPa s)
η_o — viscosity of bulk water (mPa s)
λ — ratio of solute radius to effective pore radius
σ_p — standard deviation of r_p (m)
σ_y — standard deviation of $ln\ y$
Φ — steric partition factor

Acknowledgement

The authors would like to thank the National Natural Science Foundation of China (No. 31371725), Shuguang Program supported by Shanghai Education Development Foundation and Shanghai Municipal Education Commission (No.15SG28), and the National High Technology Research and Development Program of China (863 Program) (No. 2014AA021202 and 2014AA021005), and the Fundamental Research Funds for the Central Universities (No.222201717026) for their financial support.

References

[1] Y.M. Feng, X.L. Chang, W.H. Wang, R.Y. Ma, Separation of galacto-oligo saccharides mixture by nanofiltration, J. Taiwan. Inst. Chem. Eng., 40 (2009) 326–332.
[2] J.F. Lopes, E.M.S.M. Gaspar, Simultaneous chromatographic separation of enantiomers, anomers and structural isomers of some biologically relevant monosaccharides, J. Charmatogr A, 1188 (2008) 34–42.
[3] J.W. Lee, T.O. Kwon, I.S. Moon, Adsorption of monosaccharides, disaccharides, and maltooligosaccharides on activated carbon for separation of maltopentaose, Carbon, 42 (2004) 371–380.
[4] A.A. Ghfar, S.M. Wabaidur, A. Yacine Badjah Hadj Ahmed, Z.A. Alothman, M.R. Khan, N.H. Al-Shaalan, Simultaneous determination of monosaccharides and oligosaccharides in dates using liquid chromatography-electrospray ionization mass spectrometry, Food. Chem., 176 (2015) 487–492.
[5] M. Cheryan, Ultrafiltration and Microfiltration Handbook, Technological Public Company Inc., Lancaster, USA, 1998, pp. 98.
[6] H.T. Liu, L.M. Zhao, L.Q. Fan, L.H. J, Y.J. Qiu, Q.M. Xia, J.C. Zhou, Establishment of a nanofiltration rejection sequence and calculated rejections of available monosaccharides, Sep. Purif. Technol., 163 (2016) 319–330.
[7] B. Van der Bruggen, J. Schaep, D. Wilms, C. Vandecasteele, Influence of molecular size, polarity and charge on the retention of organic molecules by Nanofilltration, J. Membr. Sci., 156 (1999) 29–41.
[8] A.K. Goulas, P.G. Kapasakalidis, H.R. Sinclair, R.A. Rastall, A.S. Grandison, Purification of oligosaccharides by nanofiltration, J. Membr. Sci., 209 (2002) 321–335.
[9] M. Nilsson, G. Trägårdh, K. Östergren, The influence of sodium chloride on mass transfer in a polyamide nanofiltration membrane at elevated temperatures, J. Membr. Sci., 280 (2006) 928.
[10] J.Q. Luo, Y.H. Wan, Effects of pH and salt on nanofiltration-a critical review, J. Membr. Sci., 438 (2013) 18–28.
[11] Y.H. Weng, H.J. Wei, T.Y. Tsai, W.H. Chen, T.Y. Wei, W.S. Hwang, C.P. Wang, C.P. Huang, Separation of acetic acid from xylose by nanofiltration, Sep. Purif. Technol., 67 (2009) 95–102.
[12] E. Sjöman, M. Mänttäri, M. Nyström, H. Koivikko, H. Heikkilä, Separation of xylose from glucose by nanofiltration from concentrated monosaccharide solutions, J. Membr. Sci., 292 (2007) 106–115.
[13] V.A. Botelho-Cunhaa, M. Mateusa, J.C.C. Petrus, M.N. de Pinhoa, Tailoring the enzymatic synthesis and nanofiltration fractionation of galacto-oligosaccharides, Biochem. Eng. J., 50 (2010) 29–36.
[14] R. José Augusto, P. António, D.P. Maria Norberta, A. Maria Diná, Sugars and lignosulphonates recovery from eucalyptus spent sulphite liquor by membrane processes, Biomass. Bioenerg., 33 (2009) 1558–1566.
[15] G.K. Athanasios, K.G. Petros, S.R. Haydn, R.A. Robert. G.S. Alistair, Purification of oligosaccharides by nanofiltration, J. Membr. Sci., 209 (2002) 321–335.
[16] R.C. Kuhn, F. Maugeri Filho, V. Silva, L. Palacio, A. Hernández, P. Prádanos, Mass transfer and transport during purification of fructooligosaccharides by nanofiltration, J. Membr. Sci., 365 (2010) 356–365.
[17] H.A. Gulec, A. Topacli, C. Topacli, N .Albayrak, M. Mutlu, Modification of cellulose acetate membrane via low-pressure plasma polymerization for sugar separation applications: Part I. Membrane development and characterization, J. Membr. Sci., 350 (2010) 310–321.
[18] B. Virginie, R.D.B. Hélène, G. Sylvain, Relationship between volumetric properties and mass transfer through NF membrane for saccharide or electrolyte system, J. Membr. Sci., 390–391 (2012) 254–262.
[19] S.N. Zhang, J.C. Zhou, L.Q. Fan, Y.J. Qiu, L.H. Jiang, L.M. Zhao, Investigating the mechanism of nanofiltration separation of glucosamine hydrochloride and N-acetyl glucosamine, Biores. Bioprocess, 3 (2016) 34.
[20] H. Xiao, H.F. Zhao, R.J. Yang, W.B. Zhang, W. Zhao, Coupled model of extended Nernst–Planck equation and film theory in nanofiltration for xylo-oligosaccharide syrup, J. Food. Eng., 100 (2010) 302–309.
[21] K. Yoshiaki, M. Kentaro, O. Tatsuo, Y. Toshiro, H. Masahiko, O. Tomomi, S. Takuji, Effect of molecular shape on rejection of uncharged organic compounds by nanofiltration membranes and on calculated pore radii, J. Membr. Sci., 358 (2010) 101–113.
[22] W.R. Bowen, A.W. Mohammad, N. Hilal, characterization of nanofiltration membranes for predictive purpose-use of salts, uncharged solute and atomic force microscopy, J. Membr. Sci., 126 (1997) 91–105.
[23] W.R. Bowen, J.S. Welfoot, Modelling of membrane nanofiltration—pore size distribution effects, Chem. Eng. Sci., 57 (2002) 1393–1407.
[24] W.R. Bowen, J.S. Welfoot, Modelling the performance of membrane nanofiltration—critical assessment and model development, Chem. Eng. Sci., 57 (2002) 1121–1132.
[25] K.Y. Wang, T.S. Chung, The characterization of flat composite nanofiltration membranes and their applications in the separation of Cephalexin, J. Membr. Sci., 247 (2005) 37–50.
[26] B. Van der Bruggen, C. Vandecasteele, Modelling of the retention of uncharged molecules with nanofiltration, Water. Res., 36 (2002) 1360–1368.
[27] H.Y. Huang, H. Zong, B. Shen, H.F. Yue, G.L. Bian, L. Song, QSAR analysis of the catalytic asymmetric ethylation of ketone using physical steric parameters of chiral ligand substituents, Tetrahedron, 70 (2014) 1289–1297.
[28] W.J. Conlon, S.A. McClellan, Membrane of softening: treatment process comes of age, J. Am. Water. Works. Assoc., 81 (1989) 47–51.
[29] T.T. Soga, M.M. Serwe, Determination of carbohydrates in food samples by capillary electrophoresis with indirect UV detection, Food. Chem., 69 (2000) 339–344.
[30] S.A. Galema, H. Hoeiland, Stereochemical aspects of hydration of carbohydrates in aqueous solutions. 3. Density and Ultrasound Measurements, J. Phys. Chem., 95 (1991) 5321–5326.
[31] P.M. Collins, R.J. Ferrier, Monosaccharides Their Chemistry and Their Roles in Natural Products, JohnWiley & Sons, Chichester, England, 1995, pp. 18.